Computer simulations of the breakup of colloid aggregates

A. H. L. West,[1,*] J. R. Melrose,[2,†] and R. C. Ball[1]
[1] *Theory of Condensed Matter and* [2] *Polymer & Colloids, Cavendish Laboratory, University of Cambridge, Madingley Road, Cambridge CB3 0HE, United Kingdom*
(Received 22 October 1993; revised manuscript received 21 December 1993)

Computer simulations of the breakup of thermally stable, fully flocculated colloidal gels were performed in monolayers under shear flow. The study was of the transient response and breakup of the aggregate gels under applied strain, and their relation to the angular rigidity of the colloidal bond. The evolution of the stress showed a power law behavior which is interpreted by scaling arguments. A scaling theory is presented for the behavior in arbitrary dimensions. In our simulations the failure of individual colloidal bonds was monitored, and for bonds with angular rigidity the dominant mode was found to be bending failure aggravated by tension.

PACS number(s): 82.70.Dd, 64.60.Ak, 05.40.+j

I. INTRODUCTION

Colloid aggregates form a component of many complex fluids such as paints [1], drilling muds, and milk products [2]. The rupture, breakup, and microrheology of such aggregates have been of recent interest theoretically [3,4], measured experimentally [5–9], and studied by simulations [10–12]. This paper concerns the rupturing of aggregate gels (i.e., aggregates which are infinitely connected) under applied shear. When a constant shear rate is applied from rest, typical behavior is that the stress builds up to a rupture point, beyond which the sample relaxes towards a shear rate dependent steady state.

The detailed behavior can be expected to depend on the form of the basic colloidal bond, and in particular whether the bond is that of a central potential with no resistance to bending moments or whether the bond possesses angular rigidity due to noncentral forces. We investigated this behavior with computer simulations of aggregates restricted to a monolayer. A technique was developed to simulate systems with colloid bonds displaying some degree of angular rigidity. Although the question of the influence of angular rigidity has been an important part of previous theories [13,3,4] it has only been included in a few simulation studies [11]. In many real systems the role of noncentral forces and hence angular rigidity is an open question. Motivated by the simulation results we report a scaling theory for the transient response which makes predictions for arbitrary dimensions of space d. It is hoped that these predictions will be compared with experiments across a variety of systems.

The rest state of aggregates is relatively well understood [14]. Aggregates at rest form, at sufficiently high monomer concentration, infinite gels which have structure varying on different length scales R. At short length scales $R < a$ the aggregate will be dense out to a grain size or strand thickness a, whereas for $a < R < \xi$ a fractal regime exists in which the density decreases from that at the grain size via a power law, $(R/a)^{D-d}$, where D is the fractal dimension and d is the dimension of space. At and beyond the scale ξ, the density correlation length, the density merges into the ambient monomer concentration and becomes homogeneous. The length ξ can be thought of as the length scale at which individual fractal clusters grew into themselves during the aggregation. A second length, the connectivity length $\chi > \xi$, determines the crossover of the connectivity to homogeneity [3]; if the aggregate is considered to be a matrix with holes, then χ can be interpreted as the upper length scale of the holes.

In the simplest models [14] colloidal particles aggregate under random motion and form angularly rigid, irreversible bonds at first contact. In these models the grain size is that of the particles, the fractal regime consists of loopless fractal strands, and the connectivity length scale χ is effectively infinite. Strong aggregates, such as those of metal sols, formed under the attractive force of the deep van der Waals minima ($E < -100k_BT$) best conform to these models. This deep potential well is likely to give rise to surface deformation and a contact zone across which bonds develop angular rigidity [6]. The small angular compliance is nevertheless crucial for the system to form loops and have a finite connectivity length.

Weaker aggregates exist where the individual bonds between colloidal particles are of the order $-10k_BT$. These particles are stabilized against aggregation in the primary minima by coating and/or charge stabilization. Attractive interactions are provided by a variety of mechanisms: depletion forces due to mixture with another smaller colloid or polymer component [7,15,16], secondary minima in the Derjaguin, Landau, Verwey, and Overbeek (DLVO) potential [17], mixture with a bridging polymer matrix [8], and the interactions of casein micelles [18]. For perfectly spherical particles with hard cores, only the latter two of these mechanisms will give angular rigidity to individual bonds. Real particles, how-

*Present address: Department of Physics, University of Edinburgh, James Clerk Maxwell Building, The King's Buildings, West Mains Road, Edinburgh EH9 3JZ, U.K.
†To whom all correspondence should be addressed.

ever, are often aspherical and/or rough on the scale of their contact zones and their coatings may not be homogeneous, all leading to some angular rigidity even for the first two mechanisms. The relative weakness of the bonds may allow consolidation of the structure during and after aggregation. External fields such as gravity, convection, or Brownian (thermal) motion move the structure during aggregation and bring it further into contact with itself [19–21]. Consolidation may increase the effective grain size of the aggregates and may also introduce loops in the structures on all scales.

Observed on length scales within the elastic fractal regime $R < \chi$, the elastic properties of an aggregate are anticipated to obey power laws. Theories for the exponents of these exist in the case of loopless fractals [13], but are an open question in the case of fractals with loops on all scales [21].

Theories of the rheological implication of the rupture of fractal aggregates have recently been reported [3,4,11]. Strain itself may act to consolidate an aggregate. Wessel and Ball [3], in particular, draw a contrast between *brittle* failure under strain in which aggregates rupture before they touch themselves and *work hardening* under strain in which aggregates make contact, form new bonds and hence reinforce the structure before rupture occurs. The rupture and agglomeration of the aggregates has an important influence on the steady state rheology and although we are a long way from a definitive understanding of this, many models have been proposed [4,11,22]. Less work has been published on the transient response [10].

Computer simulations are reported below. Previous simulations have played an important role in elucidating the structure of colloid aggregates at rest [14]. Their application, however, under nonequilibrium conditions is limited by our present inability to simulate dynamically systems with many-body hydrodynamic interactions. Several studies have considered the flow fields around static aggregates [23,24]. More recently others [10–12] have avoided the full dynamical problem by simplifying to free-draining hydrodynamics, and the present work also makes this severe approximation. Doi and Chen [10] have investigated a sticky sphere model with emphasis on the shear induced aggregation of a configuration initially dispersed at rest. They solve equations of motion with a no-slip condition at particle contacts. Potanin [11] has applied free draining flow fields to individual fractal aggregates with the aim of studying the shear dependence of the size of the aggregates. Torres, Russel, and Schowalter [25] have investigated aggregation under flow for irreversible bonded aggregates. In contrast to these works, this paper reports the application of shear to particle systems previously aggregated at rest into a fully gelled state. One of us has previously studied [12] such systems with central forces in three-dimensional simulations with emphasis on the steady state rheology and structure. Here the simulations will be of monolayers and emphasis will be on the behavior through the initial shear induced rupture of the gel structure at relatively low shear rates.

II. RIGID BONDS AND SIMULATION TECHNIQUES

Colloid potentials which possess a degree of angular rigidity have been developed [13], and one computational strategy would be to record the intial contact point between particles during aggregation and to introduce bending forces accordingly. To avoid the associated computational penalties of tracking angles, this work introduces a different approach by considering the basic colloid unit to be a stiff trimer of three spheres tightly bound together.

The interactions between trimers, the basic colloidal bond, were taken as a superimposition of 3×3 sphere pair interactions each given by a combination of a depletion well potential [15,16] and a steep power-law repulsive core ($n = 36$):

$$\frac{U_{ij}}{k_B T} = Q\left[l^2\left(\frac{r_{ij}}{d_0}\right) - \frac{1}{3}\left(\frac{r_{ij}}{d_0}\right)^3 - \frac{2}{3}l^3\right]\Theta(ld_0 - r_{ij}) + \left(\frac{r_{ij}}{d_0}\right)^{-n}, \quad (1)$$

where r_{ij} is the separation of the spheres i and j, d_0 the diameter of the core of a sphere, $\Theta(x)$ the step function, Q the interaction strength, l the range of the potential, k_B the Boltzmann constant, and T the absolute temperature.

The physical origin of the depletion potential [15] is not crucial to the present work; the potential was chosen based on past experience [12] as a finite short range potential that gave the desired binding energies and range with $Q = 131.25$ and $l = 1.2$. The bond energy, yield forces, and yield bending moments for this bond between two trimers were obtained numerically and are summarized in Table I.

Internally trimers themselves were held together by a

TABLE I. Properties of the trimer potentials for Q=131.25, l=1.2, and B=400; r_{eq} is the equilibrium bonding distance, F_y and r_y are the force and separation to break the trimer bond. Γ_y is the yield bending moment. For convenience, we give the results for the yield force in both dimensionless units systems possible—scaling by k_BT (Brownian units) and scaling by the yield force of a single particle bond $F_0 = f(r^*)$ (Stokesian units). Henceforth, all results will be given in Stokesian units, if not otherwise stated.

Bond	Rigidity	U_{min} (k_BT)	r_{eq} (d_0)	F_y (k_BT/d_0)	F_y (F_0)	r_y (d_0)	Γ_y (F_0)
bb(3)	yes	−15.37	1.446	89.5	2.32	1.506	0.699
bb(2)	yes	−10.24	1.479	77.2	2.00	1.536	0.828
fb(2)	no	−10.24	1.628	69.5	1.82	1.691	
ff(1)	no	−5.12	1.972	38.6	1.00	2.000	

judicious combination of depletion, power-law repulsion, and Hookean spring forces. The potential acting between a pair of spheres within the same trimer was

$$\frac{U_{ij}^{\text{bond}}}{k_B T} = Q\left[l^2\left(\frac{r_{ij}}{d_0}\right) - \frac{1}{3}\left(\frac{r_{ij}}{d_0}\right)^3 - \frac{2}{3}l^3\right]\Theta(ld_0 - r_{ij}) + \left(\frac{r_{ij}}{d_0}\right)^{-n} + \frac{B}{2}\left[\left(\frac{r_{ij}}{d_0}\right) - \frac{r_{\text{eq}}}{d_0}\right]^2, \quad (2)$$

with the depletion potential as above, a softer core ($n = 12$) and a Hookean spring force with $B = 400$ whose equilibrium separation $r_{\text{eq}} = 0.854\,d_0$ matches that of the combined depletion potential and soft core. With this strength and the relatively soft core repulsion, the spheres in the trimer overlapped somewhat but the trimer formed a unit with about the same stiffness as bonds between trimers. Length scales in the simulation were normalized to the diameter d_0 of the spheres. However, the area fraction was corrected for the equilibrium overlap of the spheres in the trimer.

Forces and moments were normalized by a characteristic force defined as the yield force, $f(r^*)$, of a single sphere-sphere bond. The nature of the resulting trimer-trimer bond depends on the bonding configuration; Fig. 1 illustrates and introduces a notation for the possible configurations. With the present strength of interaction only the bb(3) bond is thermally stable between a pair of trimers, the others eventually forming a bb(3) bond if subjected to Brownian motion. Only two of the possible bonding configurations, bb(3) and bb(2), exhibit angular rigidity. This fails under a sufficient pure bending moment, whereupon the bond *buckles* to a configuration without angular rigidity. This failure is *aggravated*, that is occurs earlier, if the bond is simultaneously under tensile loading and for sufficient tension complete rupture results. All of this behavior can be summed up in terms of a *yield locus* in the plane of bending moment and tension.

For comparison with the trimer behavior, we have also made simulations with simple spherical particles aggregating via the central potential (1). This provided a reference system without any angular rigidity in its bonding. Henceforth, we will refer to trimer aggregates and particle aggregates; for the former the individual bonds may possess angular rigidity whilst for the latter they do not.

Aggregation of the systems at rest were performed by use of a smart Monte Carlo technique [26]. A disordered system of trimers was produced with the trimer-trimer attraction turned off, then the attraction was turned on and the aggregation followed until a single aggregate gel spanning the periodic simulation system was produced (taking around 350 000 Monte Carlo steps per sphere for an area fraction, $\phi_a = 0.375$, where the root mean square displacement of one step in each dimension was 0.015 particle diameter). Once a gel was formed the system was thermally consolidated via further Monte Carlo steps (around 150 000 steps). Attempts were also made to aggregate the system by use of uncorrelated Brownian motion, but the small time steps required by this technique led to unacceptably long computation times. We have concentrated on simulations with area fraction ϕ_a=0.375; this was chosen to give a reasonable density correlation length ξ in relation to the sizes of sample which were practical to simulate, 128–1058 trimers.

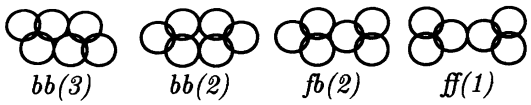

FIG. 1. Bonding configurations of trimers: base and face stands for the side of the trimer used for the bond. The number in brackets denotes the number of particle bonds between the spheres of the two bonded trimers.

To simulate the system under fixed shear rate, a free draining or "Rouse" simulation technique was used. This technique has been extensively described elsewhere [12,27]. The algorithm assumes time and length scales of interest such that inertia of the colloid particles can be ignored and the particle motion is determined by a position Langevin equation. Hydrodynamic interactions are ignored, each sphere being located in its own background fluid and experiencing a drag from the flow of this fluid. Brownian forces may also be included, but were excluded for simplicity in many of the studies below. The system is periodic with shear imposed through the background fluid forces on each particle and sliding boundary conditions. The potential in the trimer (2) was such that the distortion of trimers in shear flow remained below 0.2 sphere diameters for all shear rates for which results are reported. The shear stress $\mathbf{S}_{xy}$ in the system was calculated from the particle-particle interaction:

$$\langle \mathbf{S}_{xy} \rangle_V = -\frac{1}{V}\sum_{i=1}^{N}\sum_{j=i+1}^{N} \boldsymbol{r}_{ij}^x \boldsymbol{F}_{ij}^y, \quad (3)$$

where V is the volume of the computational unit cell and the shear gradient is applied down the y direction, i.e., $\boldsymbol{r}_{ij}^x$ is the x component of the distance vector between particles i and j, $\boldsymbol{F}_{ij}^y$ is the y component of the colloidal interaction force vector between the two particles.

Whilst the aggregation simulations were carried out relative to a heat bath, allowing some thermal consolidation, the flow simulations were not. The latter lead to different natural units which need to be explained carefully.

In Stokesian simulations of sheared aggregates without Brownian forces, the physics is determined solely by the competition between the colloidal interaction and friction forces relative to the background flow. A single parameter, W, determines the physics of this Stokesian limit and is defined here as follows.

It is clear that a bond between a pair of particles is subject to the highest elongational tension when the line between their centers lies on the extensional axis of the flow. The force increases with the separation of the particles and the bond finally breaks if the elongational force is higher than the maximum attractive force of the bond $f(r^*)$ at the separation r^*. We therefore can relate the two forces:

$$f_{\text{shear}} = \dot{\gamma}\cos\left(\frac{\pi}{4}\right) r^*\alpha = \frac{r^*}{\sqrt{2}}\alpha\dot{\gamma}\,,$$
$$f_{\max} = f(r^*)\,,$$

and define

$$W := \frac{f_{\text{shear}}}{f_{\max}} = \frac{1}{\sqrt{2}}\frac{r^*}{f(r^*)}\alpha\dot{\gamma} = \frac{3\pi}{\sqrt{2}}\mu d_0\frac{r^*}{f(r^*)}\dot{\gamma}\,, \tag{4}$$

where $\alpha = 3\pi\mu d_0$ is the Stokesian drag coefficient of a single particle and μ the viscosity of the solvent. We interpret W as a dimensionless shear rate; it is the only relevant dimensionless parameter for pure Stokesian dynamics without Brownian forces. A similar parameter is known from electrorheological fluids, where the ratio of the forces due to the flow and the electromagnetic interactions is called the Mason number [28].

We introduce a time scale τ_f defined as the time by which a sphere displaces its diameter d_0 in a viscous medium of viscosity μ under the characteristic force $f(r^*)$ neglecting inertia:

$$\tau_f := \frac{\alpha d_0}{f(r^*)}\,. \tag{5}$$

All times are given in units of τ_f if not otherwise stated. Similarly the interparticle shear stress $\mathbf{S}_{xy}$ is normalized by $\mathbf{S}^0_{xy} = f(r^*)/d_0^2$.

It is relevant to ask how the Stokesian simulations might relate to simulations which include Brownian motion. Given a potential such as (1) with absolute units we may determine the absolute shear rate $\dot{\gamma}$ above which the assumption of negligible Brownian forces relative to the flow forces is valid. The characteristic dimensionless ratio for this is known as the Péclet number, Pe, and is defined here as

$$\text{Pe} := \dot{\gamma}\tau_B = \frac{3\pi\mu d_0^3\dot{\gamma}}{8k_BT}\,, \tag{6}$$

where μ the viscosity of the solvent and τ_B is the time scale characteristic of the Brownian motion defined by $d_0^2/4 = 2D_0\tau_B$, where $D_0 = k_BT/(3\pi\mu d_0)$ is the Stokes-Einstein diffusion constant.

For the magnitude of the potential chosen in Eq. (1) we evaluated $f(r^*)$ for a single sphere-sphere bond and using Eqs. (4) and (6) we find that

$$\text{Pe} = 6.55\,W\,. \tag{7}$$

If we consider the flow simulations as those of a system characterized by forces of magnitude Eq. (1), for $W \ll 0.15$ the Brownian forces are no longer negligible with respect to the flow forces. It is not clear that this sets an absolute limit to the validity of the Stokesian simulations for Brownian systems. Empirically we found that including Brownian forces made little qualitative difference to the results down to $W \approx 10^{-2}$, except that severe fluctuations in the measured stress occurred. The simulations reported below were performed on DEC AXP 3000 workstations.

III. RESULTS OF THE SIMULATIONS

A. Aggregation

We aggregated an ensemble of seven aggregate gels with 512 trimers (N_t=512) at ϕ_a=0.375, six of which successfully formed a spacefilling network. We further aggregated two gels each at N_t=128, N_t=288, and N_t=1058 to be able to check for system size effects. We also aggregated gels of 512 particles (N_p=512) with the central potential (1).

The fractal dimension D of the clusters and the crossover length scale ξ were measured by integrating the radial distribution function $G(r)$ and plotting $[2\pi\int G(r)r\,dr]$ against r on a log-log scale. Figure 2 shows an example. Above a crossover length scale ξ the slope of the curves changed from values $D < 2$ to $D = 2$. For $r < \xi$, D (calculated using linear regression) ranged from 1.70 to 1.73 for the different aggregates with $\xi \approx 9.5$ to 10.5. No system size dependence of D or ξ was observed, even though for the smallest N_t=128 aggregates ξ reached about 40% of the box side length L. The fractal dimension of the particle aggregates were higher than of the trimer aggregates (D=1.74±0.04; $\xi = 7\pm1$), most likely because the central bond allows a greater degree of consolidation. The crossover lengths for the trimer and particle cases, however, are about the same if we rescale ξ by the appropriate bond distance.

Figure 3 shows the fully aggregated configuration (a) of a trimer sample $N_t = 1058$ (No. 1) compared with that (b) of a particle sample $N_p = 512$ (No. 1). We find that both structures are consolidated with loops on all scales within the fractal regime and a grain size of 2–3 particle or trimer diameters. We sometimes find rather dense structures at the tips of clusters which we attribute to thermal consolidation by the Monte Carlo selection.

In the trimer aggregates the restructuring process generally leads not only to denser but also to more rigid structures consisting of bb(3) bonds. Nevertheless we also find fb(2) and ff(1) configurations in the aggregates.

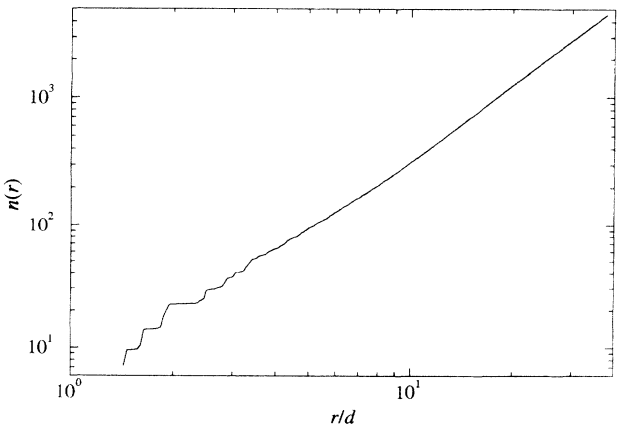

FIG. 2. $n(r) := 2\pi\int G(r)r\,dr$ vs r on a log-log scale for the aggregate gel, N_t=1058 (No. 1), at ϕ_a=0.375 reveals $D = 1.72 \pm 0.02$ and $\xi \approx 10$—the crossover can be seen by the kink in the curve.

Most of these bonds are found in dense regions where local overcrowding, i.e., lack of space to form more bonds, took place. We refer to these and other bonds which do not lie on the elastic backbone on the aggregate as *minor* bonds. Conversely we refer to a single bond which interconnects two clusters at a *junction* as a *vital* bond. Usually vital bonds possess angular rigidity, but occasionally we find a vital fb(2) or ff(1) bond, which makes the strand as a whole unable to transmit a bending moment.

It might be thought that the trimer bonds with angular rigidity would inhibit consolidation and the formation of loops. However, up to the connectivity length scale χ (which we observed to be 2–3 ξ), the aggregates have loops on all scales and as will be reported below the exponents for the compliance in the fractal regime are not the same as predicted by simple theories of loopless fractals [13]. Aggregation events usually start by two clusters sticking at one contact which even with trimers may not possess angular rigidity, leaving the resulting branches free to rotate until they stick at a second point, forming a loop and stabilizing the structure.

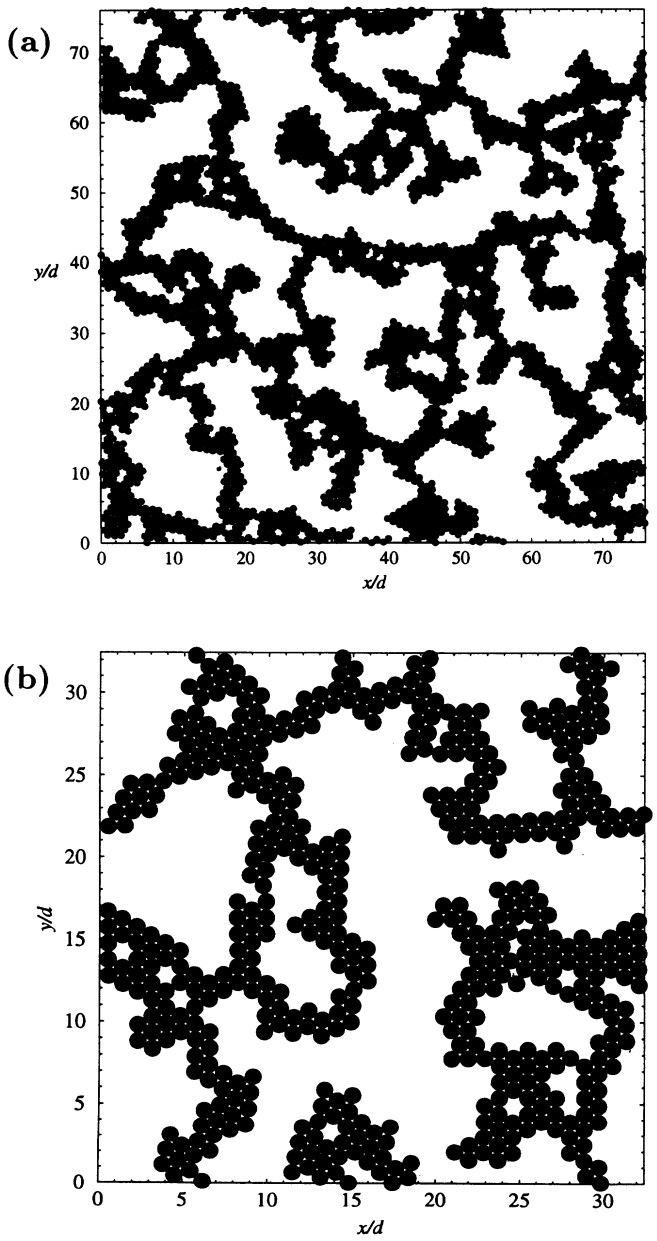

FIG. 3. Aggregated trimer sample N_t=1058 (sample No. 1) (a) and particle sample N_p=512 (No. 1) (b) at $\phi_a = 0.375$ after 500 000 Monte Carlo steps.

B. Stress evolution of gels in shear flow

We first report on a bulk property of the aggregates under shear: the behavior of the interparticle shear stress $\mathbf{S}_{xy}$ as a function of strain γ and shear rate W. The gels rupture when the stress reaches a maximal yield value beyond which it relaxes to lower values. The aggregates were sheared with shear rates extending over several orders of magnitude, corresponding to $W = 1.526\times10^{-4}$ to 1.526, up to strains usually of γ=0.42 which was beyond the yield point in all cases.

Figure 4 shows the interparticle shear stress $\mathbf{S}_{xy}/\mathbf{S}^{o}_{xy}$ against the strain γ for different aggregates at a medium shear rate, $W = 1.526\times10^{-1}$. We observed sample variations which were sensitive to the applied shear rate. The largest sample variations were found in runs under very low shear rates. Over the range of sizes studied, it is hard to discern systematic system size effects over the sample variation. In what follows we will rely mostly on the results of the two largest aggregates of N_t=1058, whose statistics appear superior to all others. The viscoelastic response is affected by structural defects and smaller system sizes will be more sensitive to these. In fact at the smallest system size, N_t=128, one aggregate was quite anomalous in its behavior which we attribute to defects.

We first show data for strains below the yield strain γ_y, defined as the strain of the first local stress maximum. This was the global maximum in stress, except at the lowest shear rates where the yield criterion was more ambiguous and we had to take that maximum of stress after which a "considerable" stress relaxation took place.

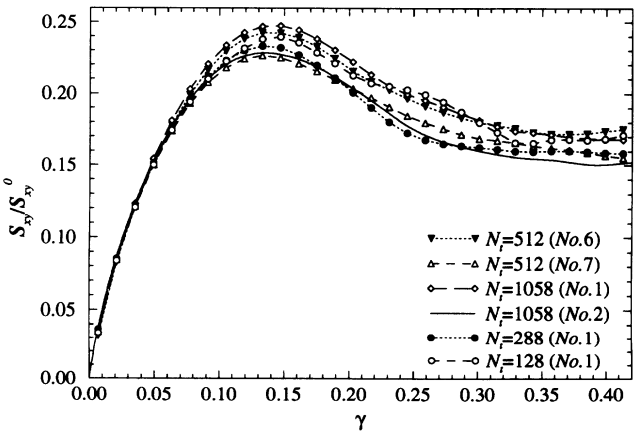

FIG. 4. Interparticle shear stress $\mathbf{S}_{xy}/\mathbf{S}^{o}_{xy}$ vs strain γ at a medium shear rate, $W = 1.526\times10^{-1}$, for different aggregates (see legend). Variations between different aggregates of the same system size are small but evident.

Figure 5 shows a plot of the interparticle stress $\mathbf{S}_{xy}/\mathbf{S}^0_{xy}$ against strain γ on a logarithmic scale for the aggregate with $N_t = 1058$ (No. 1) subjected to a range of shear rates over many runs starting from the same initial configuration. For shear rates below $W < 2\times10^{-2}$ the plots show a significant region of pure power law behavior by

$$\mathbf{S}_{xy} \propto \gamma^{\beta}, \tag{8}$$

with $\beta = 0.62 \pm 0.01$ independent of the shear rate. The power law regime is eventually terminated at high strains γ by the yield regime—the turnover of the plots on the far right. Occasional small kinks are evident in the power law regime. At any shear rate deviations from the power law are also found for small enough strains. We will argue below that the power law regime occurs when a dynamic equilibration length scale R falls within the fractal regime. For small times the length R falls below the grain size a (the lower cutoff of the fractal regime) and the power law regime is therefore reached only above a shear rate dependent strain. For higher shear rates ($W > 10^{-1}$) the time is too short for R to reach fractal length scales even for large strains prior to yield and the pure power law regime is lost completely. We show two sets of data for these shear rates. At the higher shear rate $W = 1.526$ the slope of the stress-strain response is close to linear, which is simply the elastic response of indvidual bonds—i.e., the structure is pulled apart on the length scale of the bonds.

Figure 6 shows a plot of the interparticle stress $\mathbf{S}_{xy}/\mathbf{S}^0_{xy}$ at given fixed strain as a function of the shear rate W, where we started each run from the same initial configuration. Again we find a power law behavior of the stress:

$$\mathbf{S}_{xy} \propto W^{\epsilon}, \tag{9}$$

with ϵ=0.397 $\pm$ 0.01.

We argue below that both power law behaviors reflect that at low shear rates the gel can equilibrate the stress due to the applied strain γ up to a time-limited length scale in the fractal regime. For high shear rates the slope tends to horizontal in the limit $W \to \infty$ for small

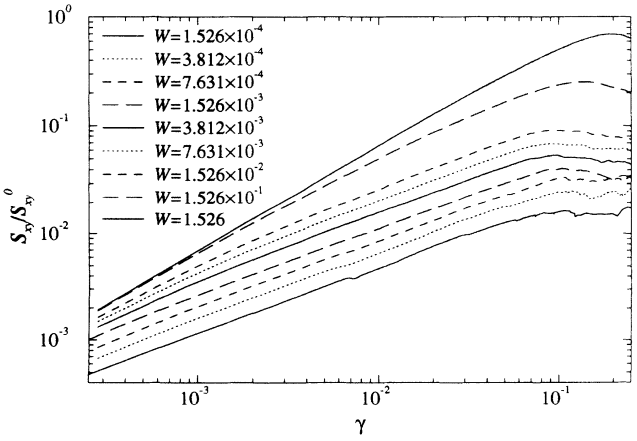

FIG. 5. Interparticle shear stress $\mathbf{S}_{xy}/\mathbf{S}^0_{xy}$ vs strain γ on a log-log scale for the aggregate with $N_t = 1058$ (No. 1) for increasing shear rates W (see legend).

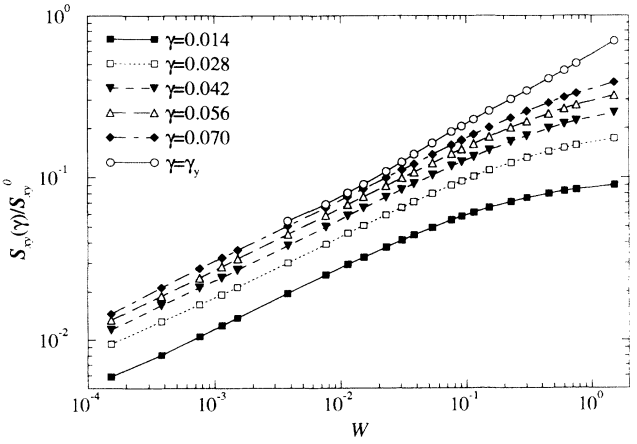

FIG. 6. Interparticle shear stress $\mathbf{S}_{xy}/\mathbf{S}^0_{xy}$ vs shear rate W for a given strain γ (see legend) on a log-log scale for the aggregate with $N_t = 1058$ (No. 1).

strains, corresponding to affine elastic response of the single colloid bonds. For larger strains the curves extend their power law behavior to higher strain rates, whereas the slope remains constant. The structure breaks when $\boldsymbol{\sigma}(\gamma_y) = \boldsymbol{\sigma}_y(W)$, where the yield strain γ_y is much more weakly a function of W than the yield stress $\boldsymbol{\sigma}_y$.

Figure 7 shows a plot of the stress $\mathbf{S}_{xy}/\mathbf{S}^0_{xy}$ against time t through the full transient region pre- and postrupture. We observe that the envelope of the stress curves for all shear rates except the highest share a universal relaxation curve beyond the stress maximum. This corresponds to a power law $\boldsymbol{\sigma} \propto t^{-\epsilon'}$ and we find that for each aggregate the measured exponent ϵ' is within errors equal to the exponent ϵ of Eq. (9). For very high shear rates the stress overshoots and drops significantly faster after rupture.

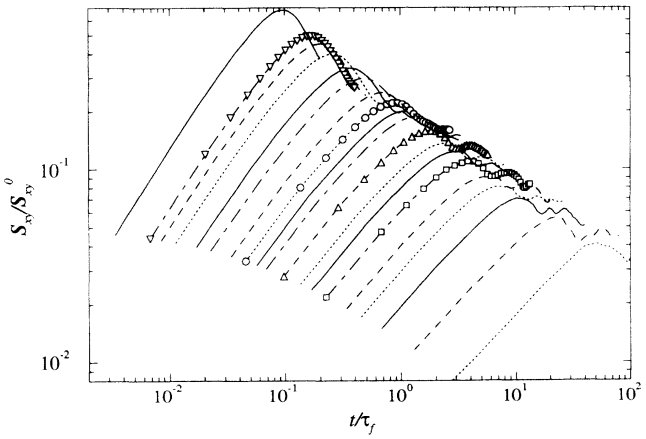

FIG. 7. Interparticle shear stress $\mathbf{S}_{xy}/\mathbf{S}^0_{xy}$ vs time t/τ_f on a log-log scale for many individual shear rates for the aggregate $N_t = 1058$ (No. 1). From right to left increasing shear rate $W = 1.526\times10^{-3}$, 3.816×10^{-3}, 7.631×10^{-3}, 1.145×10^{-2}, 1.526×10^{-2}, 2.289×10^{-2}, 3.053×10^{-2}, 3.816×10^{-2}, 5.342×10^{-2}, 7.631×10^{-2}, 9.158×10^{-2}, 1.145×10^{-1}, 1.526×10^{-1}, 2.289×10^{-1}, 3.053×10^{-1}, 4.579×10^{-1}, 6.105×10^{-1}, 7.631×10^{-1}, and 1.526. We draw symbols for a few shear rates to illustrate how the stress-strain curves fall onto a universal envelope during the elastic recovery after yield reflecting a power law behavior.

C. Scaling laws

In this section, we develop a simple scaling argument consistent with the observed power law behavior, based on the view that as time proceeds the stressed structure locally equilibrates its stress on longer and longer length scales R. We assume R to lie in the elastic fractal regime, $a < R < \chi$, and we assume that this single dynamic length scale R determines the transient response of the strained system.

Consider a fractal blob of gel of size R which is distorted by a displacement δR under a force F. If we use the most general power law ansatz for the compliance as a function of R,

$$C(R) = \frac{\delta R}{F} \propto R^{Z_c}, \tag{10}$$

the shear modulus $G(R)$ of the blob scales as

$$G(R) = \frac{\sigma}{\gamma} = \frac{F/R^{d-1}}{\delta R/R} \propto R^{-(Z_c+d-2)}. \tag{11}$$

We will for simplicity assume that the exponent Z_c is independent of the strain throughout the region of stress buildup, although in principle one should anticipate the possibility of a crossover at $R = \xi$. The time for a region of length R to equilibrate its stress is

$$\tau = \alpha(R)C(R), \tag{12}$$

where the drag coefficient $\alpha(R)$ in the free draining approximation (Rouse level) is given by

$$\alpha = 6\pi\mu Na \propto 6\pi\mu a\left(\frac{R}{a}\right)^D. \tag{13}$$

This then leads to a length-scale-dependent relaxation time

$$\tau(R) \propto R^{D+Z_c}, \tag{14}$$

and correspondingly the length scale to which stress is equilibrated over a given time is

$$R(t) \propto t^{1/(D+Z_c)}, \tag{15}$$

provided that R is smaller than the connectivity length χ.

The stress $\sigma(t)$ built up as a function of time t is that appropriate for a strained unit (blob) of linear size $R(t)$:

$$\sigma \propto G[R(t)]\gamma, \tag{16a}$$

which when combined with Eqs. (11) and (15) gives the result

$$\begin{aligned}\sigma &\propto R^{-(Z_c+d-2)}\gamma \\ &\propto \gamma t^{-\left(\frac{Z_c+d-2}{D+Z_c}\right)}.\end{aligned} \tag{16b}$$

Note, despite the negative exponent of t the stress will increase with time at a constant shear rate due to the increase in strain $\gamma(t)$. In the case of a homogenous constant shear flow with $\gamma = \dot{\gamma}t$ we can conclude

$$\sigma \propto \dot{\gamma} t^{\frac{D-d+2}{D+Z_c}}, \tag{16c}$$

$$\sigma \propto \dot{\gamma}^{\frac{Z_c+d-2}{D+Z_c}} \gamma^{\frac{D-d+2}{D+Z_c}}, \tag{16d}$$

$$\sigma \propto \dot{\gamma}^{\epsilon}\gamma^{\beta}. \tag{16e}$$

After rupture at time $t = t_y$ we assume that the aggregate consists of blobs of scale $R(t_y)$ effectively at fixed strain and relaxing their excess stress by Eq. (16b):

$$\sigma \propto \gamma_y t^{-\left(\frac{Z_c+d-2}{D+Z_c}\right)}, \tag{17a}$$

$$\sigma \propto t^{-\epsilon'}, \tag{17b}$$

and hence $\epsilon' = \epsilon$ as in the simulations. Note, this assumes that the same compliance exponent holds for the structure before and after rupture, notwithstanding the loss of the power law regime in Fig. 5 just prior to the first stress maximum.

If we use the measurements of D, ϵ, and β of the simulations and use $d = 2$ which is appropriate for simulations in a monolayer, we obtain two independent values for Z_c for $[N_t = 1058$ (No. 1)]:

$$Z_c(\epsilon) = D\frac{\epsilon}{1-\epsilon} = 1.16 \pm 0.03, \tag{18a}$$

$$Z_c(\beta) = D\frac{1-\beta}{\beta} = 1.13 \pm 0.05. \tag{18b}$$

The second aggregate $[N_t = 1058$ (No. 2)] gave

$$Z_c(\epsilon) = D\frac{\epsilon}{1-\epsilon} = 1.23 \pm 0.08, \tag{19a}$$

$$Z_c(\beta) = D\frac{1-\beta}{\beta} = 1.16 \pm 0.10. \tag{19b}$$

These low values of Z_c between 1.1 and 1.3 for the trimer aggregates are far from that for loopless fractals [13]. As noted earlier we attribute this to our fractals having loops on all length scales, stiffening the structure, increasing the angular rigidity, and decreasing the exponent Z_c.

The scaling argument introduced can also be used to determine the point at which the gel will yield, if we introduce a yield criterion and further assume that yield occurs at the characteristic length scale $R(t)$ at a single bond or junction which is weak relative to blobs of scale R. The yield stress will occur when a local bending moment or elongational force exceeds the maximum couple or force a bond can mantain. The largest local bending moments are expected to be of the order

$$\begin{aligned}\Gamma &\propto \sigma R^d \propto \dot{\gamma} t^{\frac{D+2}{D+Z_c}} \\ &\propto \dot{\gamma}\dot{\gamma}^{-\left(\frac{D+2}{D+Z_c}\right)}\gamma^{\frac{D+2}{D+Z_c}} \\ &\propto \dot{\gamma}^{\frac{Z_c-2}{D+Z_c}}\gamma^{\frac{D+2}{D+Z_c}},\end{aligned} \tag{20a}$$

so if Γ_y is the maximum bending moment a bond can bear we expect yield at the corresponding strain:

$$\gamma_y|_{\Gamma_y} \propto \dot{\gamma}^{-\left(\frac{Z_c-2}{D+2}\right)}\Gamma_y^{\frac{D+Z_c}{D+2}}. \tag{20b}$$

Similarly, the largest local bond tensions are expected to be of the order

$$F \propto \sigma R^{d-1} \propto \dot{\gamma} t^{\frac{D+1}{D+Z_c}} \propto \dot{\gamma}^{\frac{Z_c-1}{D+Z_c}} \gamma^{\frac{D+1}{D+Z_c}}, \quad (21a)$$

so if bonds break due to F exceeding the maximum bond force F_y we expect the corresponding yield strain to be

$$\gamma_y|_{F_y} \propto \dot{\gamma}^{-\left(\frac{Z_c-1}{D+1}\right)} F_y^{\frac{D+Z_c}{D+1}}. \quad (21b)$$

We can compare these theoretical predictions with the results of the simulations. It is noted that the calculation above assumes that the structure breaks at a single bond; in practice the couples and forces at yield may be, due to loops, divided up over several branches or even spread over rupture zones. Pictures of the sheared aggregates (see Sec. III D), however, do suggest that the structure breaks at *junction* zones between blobs within which the structure is loopless.

In Fig. 8 we plot on a log-log scale the yield strain γ_y against the dimensionless shear rate W for several trimer aggregates [Fig. 8(a)] and two particle aggregates [Fig. 8(b)]. We also coplot lines showing the slopes of the power law predictions of Eqs. (20b) and (21b). To generate these we have substituted the least and greatest values of Z_c backed out from the exponents of the stress curves. We divide the plot into two regimes. For $W < 10^{-1}$ we estimate that rupture occurs on fractal length scales and we expect the scaling theory to hold. In the case of the particle aggregates [Fig. 8(b)], the data is clearly consistent with the predictions of Eq. (21b); the dominant failure mechanism in the central force case without angular rigidity of the colloid bond we conclude to be tensile failure. In the case of the trimer aggregates neither of the predictions of Eqs. (20b) or (21b) are satisfactory. In the next section we report on a careful examination of the local failure modes of trimer aggregates.

In the high shear rate regime $W > 10^{-1}$, we estimate that the equilibration length falls below the short length scale cutoff a of the fractal regime and as noted above the scaling theory is not applicable in this regime. At these shear rates the critical strain increases with W and furthermore there is no qualitative difference between the particle and the trimer aggregates.

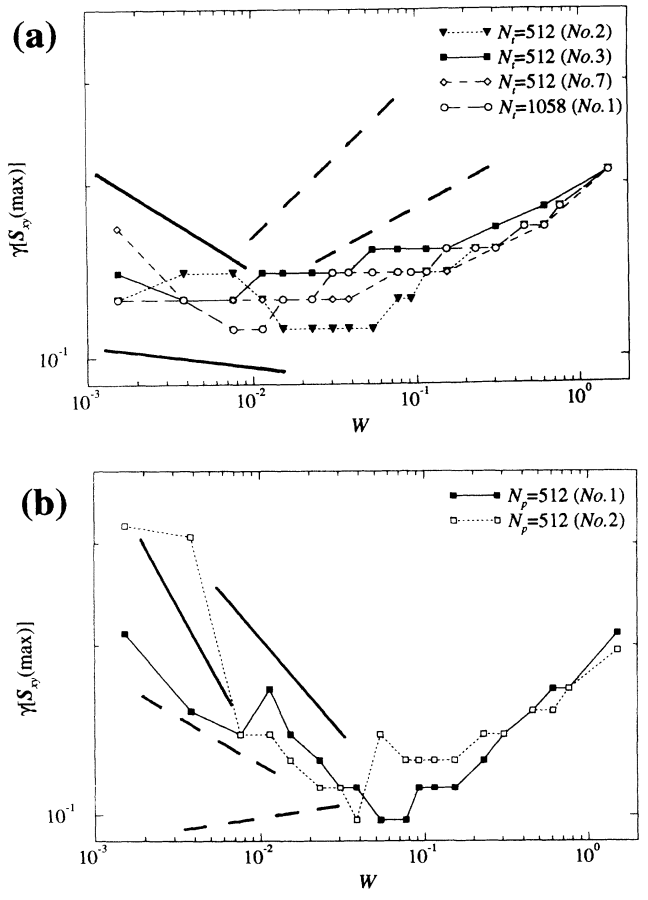

FIG. 8. Yield strain γ_y vs shear rate W on a log-log scale for trimer aggregates (a) (see legend). The yield strain γ_y remains nearly constant for low shear rates, and for two particle aggregates (b). A crossover from fractal to local length scales is observable above $W \approx 10^{-1}$. (- - -) predictions of bending failure [Eq. (20b)], (——) predictions of tensile failure [Eq. (21b)].

D. Failure modes

It is of interest to examine in detail the nature of the local rupture process in colloid aggregates. Whilst the trimer model we investigate may have some nonphysical aspects, we nevertheless feel that the following discussion may motivate understanding of real systems.

In principle four modes of failure are conceivable:

- *Tensile failure*, caused by an elongational force, F_e, larger than the yield force, F_y, of a colloidal bond.
- *Bending failure*, due to a bending moment, Γ_b, in excess of the maximum bending moment, Γ_y, a bond can bear. In our model pure bending failure will lead only to buckling, i.e., solely an angular failure, of the bond, leaving a bond weakened without angular rigidity but with a lower tensile yield force.
- *Aggravated failure*—bonds buckle at a lower bending moment, if an additional tension is present.
- *Shear failure*—a failure along the shear axis, caused by the gliding effect between two layers of trimers aligned with the shear axis. A shear failure breaks a trimer bond by consecutively removing one particle bond between two spheres at a time.

The elongational force F_e and bending moment Γ_b across individual trimer-trimer bonds were calculated from the forces $\boldsymbol{F}_{ij}$ between sphere i of the first trimer and sphere j of the second trimer. We took F_e to be

$$F_e := \left(\sum_{i,j=1}^{3} \boldsymbol{F}_{ij} \right) \cdot \hat{\boldsymbol{R}}^c, \quad (22a)$$

where $\hat{\boldsymbol{R}}^c$ is a unit vector along the line of centers (of mass) of the two trimers. For the bending moment Γ_b

we took couples with respect to the midpoint $\boldsymbol{R}^m$ of the line of centers,

$$\Gamma_b := \left| \sum_{i,j=1}^{3} \boldsymbol{F}_{ij} \times (\boldsymbol{r}_i - \boldsymbol{R}^m) \right| \mathrm{sgn}(F_e) . \qquad (22b)$$

The sign convention in Γ_b distinguishes bonds under positive tension (+) which might rupture completely, from those under tensile compression (−) which could only buckle.

We checked how sensible these definitions were by measuring them within bonds or chains of bonds subjected to known external forces or force couples. The internal measurements of (22a) and (22b) accurately reproduced the known applied values.

We gathered statistics on all breaking processes over all aggregates at low shear rates. First we identified all bonds which changed their coordination number (as per the classification of Fig. 1) between strains 0.014 and 0.42, then for these bonds we extracted the histories of F_e and Γ_b. We distinguish *breakage*, where the bond is totally disengaged, and *buckling*, where a bond just loses its angular rigidity [i.e., from a bb(3) to a fb(2) configuration]. We examined the pictures of the aggregates as a function of strain very carefully and followed the stress-strain history of broken and buckled bonds.

Figures 9 and 10 show snapshots of aggregates formed of trimers (Fig. 9) and particles (Fig. 10), both at low strain preyield [Figs. 9(a) and 10(a)] and high strain postyield [Figs. 9(b) and 10(b)]. The trimers and particles which were involved in bond buckling and/or breaking up to γ=0.42 are shown by open circles. In the case of the particle aggregates, we can see that the structure has globally deformed but is still mainly intact, i.e., no vital bond has been broken until $\gamma = 0.42$. The structure shows some "rigidity" because the form of chunks of cluster are conserved. Breaking occurred at weak zones, *junctions*, between clusters, which act as joints of the whole structure.

In the trimer case breaking and buckling also occurred at such junctions between blobs, but in contrast to the particle aggregate, more bonds have failed. The pictures suggest that stress accumulates at the junction as in the particle case, but because most of these possess angular rigidity, they do not act as flexible joints. The junctions resist deformation until the stresses are sufficient to *buckle* the junction to a configuration without angular rigidity which is then able to rotate freely. The pictures suggest that the major mode of yielding for low shear rates is bending failure although some shear failures were also evident. We can also see that almost all bonds which buckled or broke lie on one of the percolating paths of the gel. Overall, however, the aggregate still percolates because several independent percolation axes exist. At yield we observe that the length scales associated with the rupture zones, their spatial frequency and their actual size, both increase with increasing shear rate. This observation is quite compatible with the scaling theory where it was argued that the equilibration length scale at yield decreases with increasing shear rate.

We examined the failures of the individual bond types. Statistically bb(3) failures are the dominant process (55.9%) whilst failures of fb(2) and ff(1) configurations contributed 9.6% and 34.6%, respectively. The overall portion of ff(1) bonds stays about the same, the share of the fb(2) configurations rose by 1.49%, whereas the portion of bb(3) bonds fell by 1.53%.

The failure of the weakest ff(1) bonds is only possible in elongation. Their weakness determines the global tensile force level. We observed that this always occurred at an uncritical location in the aggregate, i.e., the bond broken can be classified as *minor*. Typical examples can be easily spotted in the pictures (Fig. 9).

The rupture of an fb(2) configuration can be caused

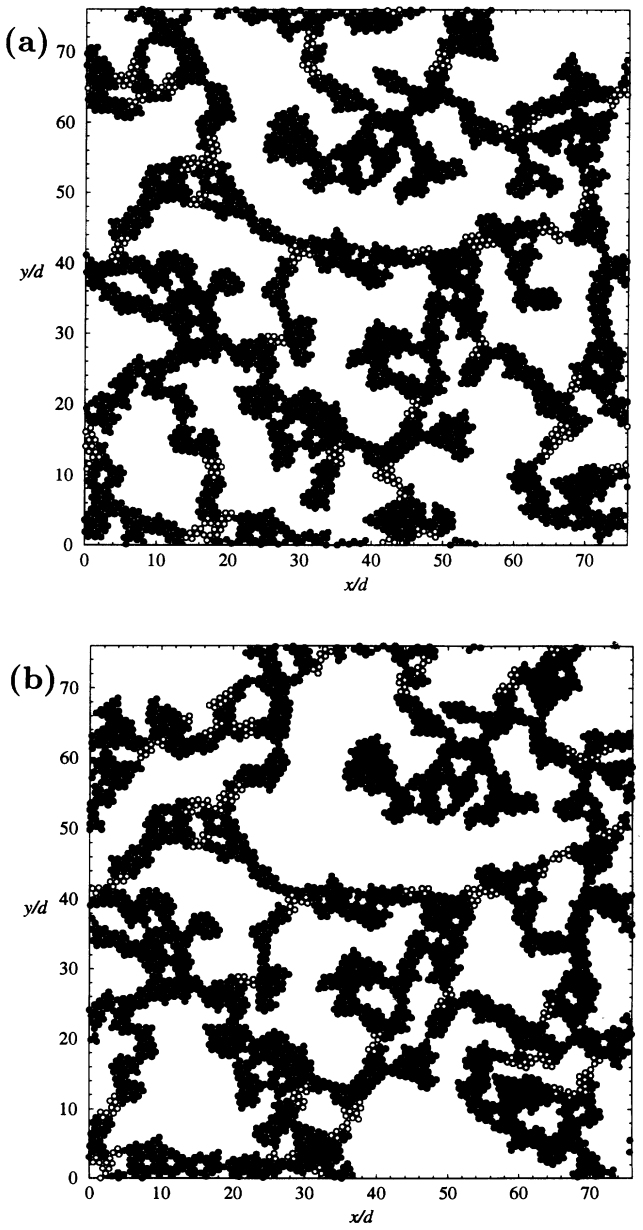

FIG. 9. A trimer aggregate $N_t = 1058$ (No. 1) strained from rest [$\gamma = 0.014$ (a)] to $\gamma = 0.42$ (b) at the lowest shear rate, $W = 1.526 \times 10^{-4}$—open trimers refer to trimers which change their initial bonding configuration, i.e., break or buckle, for $0 \leq \gamma \leq 0.42$.

by shear or by tension. Both modes were present and distinguishable, but tensile failures were more common. However, fb(2) bonds fail rather seldom, because they are strong in comparison to the ff(1) bonds and they are relatively free to evade breaking, because they can convert local deformation into global folding or unraveling of the branch. fb(2) bonds can be present in the rest structure but also are acquired under strain by the buckling of bb(3) bonds.

The strongest bb(3) bonds are broken in two stages. First, they buckle mostly due to a bending moment in combination with an applied tensile force and convert into a ff(1) or more likely fb(2) bond. Some of these conversions were also caused by pure bending, in a combination of bending with compression or by shear, whereas we found no example of failure which was solely due to tensile forces. We found that the buckling failures were almost evenly distributed over all strains, whereas the eventual second stage of the failure, consisting of the final breakage of the weakened bond in tension usually took place very late in the strain—in fact only a minority (15.8%) of buckled bonds did actually rupture for strains below $\gamma \leq 0.42$. This suggests that the principal deformation is folding and unraveling, because bonds without angular rigidity can be sustained in this kind of deformation even for large strains.

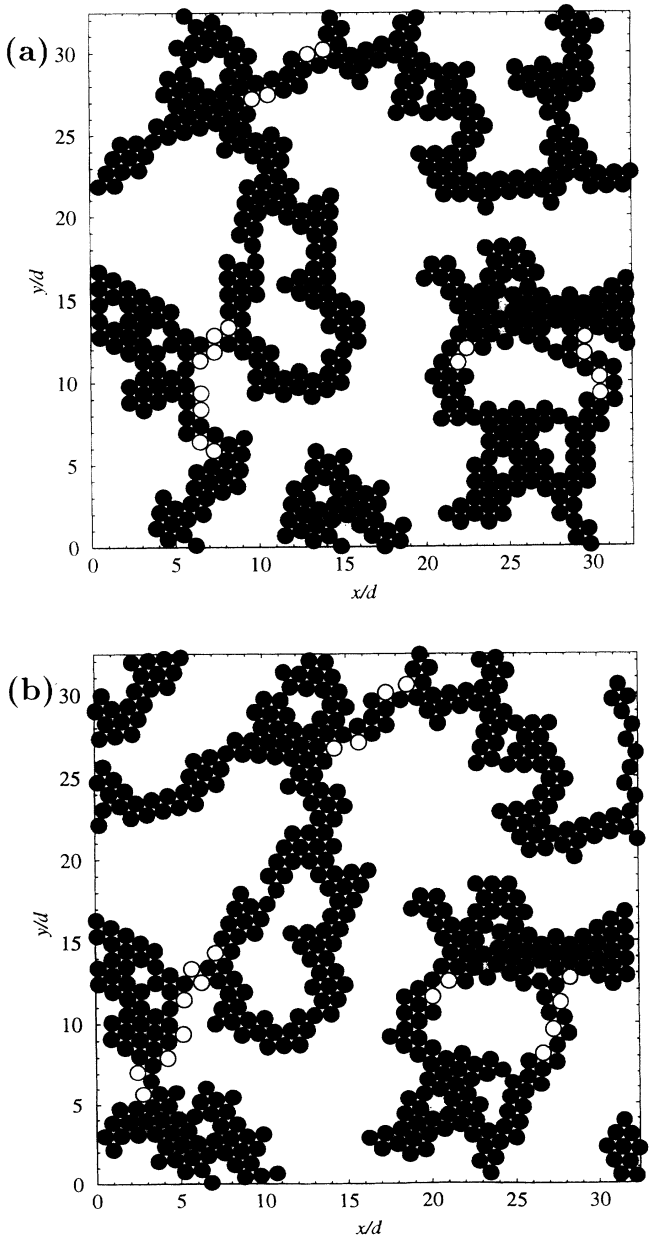

FIG. 10. A particle aggregate $N_p = 512$ (No. 1) with Q=131.25 strained from rest [$\gamma = 0.014$ (a)] to $\gamma = 0.42$ (b) at a very low shear rate, $W = 1.526\times10^{-3}$—open particles refer to particles which change their initial bonding configuration, i.e., break, for $0 \leq \gamma \leq 0.42$.

There are, however, also examples of total bb(3) breakages at low strains even before the yield stress was reached. They all fall in one class, which can be best termed *initial weak bonds*. These are bonds which are already initially far from equilibrium, often already beyond the steepest part of the potential. These bonds have in common that the bending moment was highest for the unsheared aggregate and the disengagement took place below the nominal values of F_e and Γ_b for aggravated failures.

The fact that the structure is softened by buckling and breakages of bb(3) configurations at low strains can explain the observed deviation of some aggregates from the power law for σ against γ below the yield strain. These acquired defects together with initial defects on the backbones of the gel are also the likely cause of sample variation and sensitivity of this variation to system size.

To assess the relative importance of the bending and tension in aggravated failures more closely, we also plotted bending moment against tensile force for failed bonds at their individual yield point, which we defined as the point where at least one particle bond between spheres of bonded trimers becomes unstable. The data is subject to a sampling error as the configurations were only stored at intervals. This was done for all large aggregates ($N_t \geq 512$) for two shear rates: $W = 1.526\times10^{-3}$ [Fig. 11(a)] and $W = 1.526\times10^{-4}$ [Fig. 11(b)]. For both shear rates, we see that the data is scattered around the numerical prediction of the yield locus of aggravated failure. This theoretical line was derived by applying a constant tensile force and a stepwise increasing bending moment to a single bb(3) bond until the bond yielded.

The data points above the isolated measurements may be due to the nonequilibrium nature of the rupture process during the shear of the aggregates and to the fact that bonds in the aggregates are not isolated but may be jammed. A shear failure is expected to be found in a region around $\Gamma_b \approx 0.20$ and $F_e = 1$. This region can be identified especially well at the lowest shear rate $W = 1.526\times10^{-4}$ [Fig. 11(b)]. Some of the failures also took place under compression, but most failures occur under tension. Comparing the graphs for the two shear rates, it is evident that the relative importance of bending and tension in the dominating aggravated failure mode is shear rate dependent. For the lower shear rate, $W = 1.526\times10^{-4}$, investigated, the distribution is biased to low values of the tensile force, whereas for the

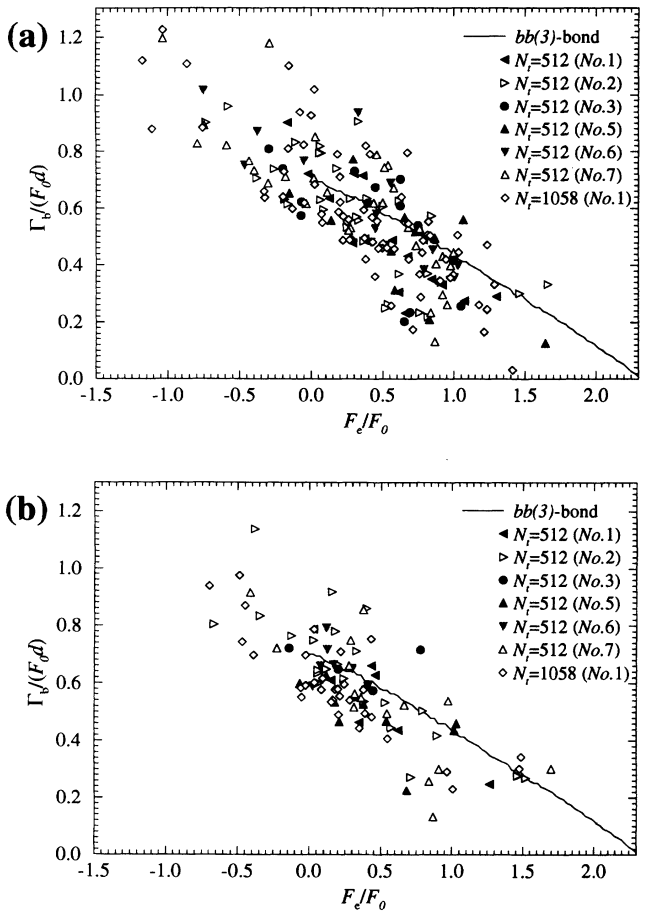

FIG. 11. Yield bending moment Γ_b/F_0 vs yield tensile forces F_e/F_0 for the transition of a bb(3) configuration to a fb(2) configuration for several aggregates at $W = 1.526\times10^{-3}$ (a) and $W = 1.526\times10^{-4}$ (b). The line in both graphs is the numerical result for the failure of an isolated bb(3) bond by external applied tension and couples.

higher shear rate, $W = 1.526\times10^{-3}$, the failures are more evenly distributed along the yield locus of an isolated bond.

IV. SUMMARY AND DISCUSSION

The aim of this work has been the understanding of the transient response of a colloid aggregate gel to an applied shear rate, with particular emphasis on the role played by angular rigidity. Computer simulations led us to a scaling law interpretation of the observed stress response.

We have constructed model aspherical colloids by use of composite units, each a trimer of tightly bound spheres whose interactions were defined by a superimposition of 3×3 pair interactions. This represents only the simplest of a wide range of composite particles which could be explored. A free draining approximation was made for the particle friction, ignoring hydrodynamic interactions.

The aggregates were grown in a monolayer by off-lattice, polydisperse diffusion limited cluster aggregation (DLCA) using a smart Monte Carlo algorithm of $O(N)$, being 14 times faster than a comparable Brownian dynamics code. We used a relatively high area fraction of ϕ_a=0.375 in order to obtain gelation well within the size range of our simulations, giving a connectivity length χ of order of 25 units. This area fraction combined with thermal consolidation causing denser structures leads to a rather high average fractal dimension (D=1.72) and a short crossover length scale ($\xi \approx 10$). The gels also contained loops on all length scales.

Shear simulations were carried out in the Stokesian limit in which Brownian motion is neglected, leaving a competition between only the particle friction and interparticle forces. In this regime a dimensionless shear rate W is the unique control parameter which we explored over several orders of magnitude. The interactions were such that as regards deformation, the aggregates were in the *brittle* regime, where fractal branches break before they can touch and reinforce the structure.

The stress exhibits power law dependence on both strain and shear rate, towards a maximum corresponding to a weakly varying yield strain. We associate the maximum with rupture in the structure, and observe a further power law for the subsequent stress relaxation with time. All of these power laws could be interpreted and related through a simple scaling theory, fitted with the scaling of the elastic compliance with length scale as the only independent exponent Z_c.

The scaling theory assumes that the transient response to the applied shear rate is dominated by a single dynamic length scale: that scale to which the stress is equilibrated by time t. Pure power laws follow where this dynamic length scales falls within the fractal regime of the aggregate. The theory is not restricted to two dimensions.

The values of the elastic compliance exponent Z_c were backed out from the data using the scaling theory, and these values were found to be consistent for three independent scaling plots. For the trimer model with angular rigidity, the two largest aggregates (N_t=1058), were consistent with $Z_c = 1.2 \pm 0.12$. This value for a fractal with loops is much lower than the predicted $Z_c \geq 3$ for loopless fractals [13]. For smaller aggregates, $N_t = 512$, values of Z_c were consistent within error bars for the three estimates, but varied between aggregates across the range 1.0 to 1.6. We argue that some aggregates with large Z_c values are softer (i.e., require less force at a given length scale to achieve the same displacement) due to defects consisting of bonding configurations lacking angular rigidity. The sample will be most sensitive to these if they occur in the rest state structure in regions that can become junction zones under strain (see below), and for the aggregate with $Z_c = 1.6$ this was confirmed by observation of the gel structure.

For the two particle aggregates with central colloid bonds consistency between the two scaling laws of the stress σ [Eq. (16e)] prior to rupture was weaker: calculating Z_c via $\sigma \propto \gamma^{\beta}$ averaged over several shear rates, we found $Z_c = 2.5 \pm 0.5$ whilst calculating Z_c via $\sigma \propto \dot{\gamma}^{\epsilon}$ at constant strain, we found $Z_c = 1.9 \pm 0.1$. The higher values relative to the trimer case reflect the softness of the particle aggregate structure. The particle aggregates,

however, showed a "collective rigidity" by keeping large parts of the structure undeformed post rupture.

For the tenuous gel structures, stress equilibration leads to stress concentration in weak zones which form junctions in the structure lying between stronger blobs. It is in these zones that rupture takes place. As the shear rate increases rupture occurs at shorter and shorter equilibration length scales—the distance between rupture zones decreases whilst the size of the zones themselves increases. At the highest shear rates the equilibration scale at rupture falls below the short range cutoff to the fractal regime: in effect no equilibration before rupture occurs and the structure is pulled apart at the shortest length scales. The scaling theory was extended to the rupture itself by adopting yield criterion in the zone, either failure under tension or bending. For the case of the particle aggregates the failure under tension criterion was consistent with the yield strain against shear rate data. For the case of the trimer aggregates [Fig. 8(a)], however, neither criterion could be concluded consistent (see below).

An investigation was made of the local rupture of the trimer aggregates. We identified a mode of aggravated failure in which bonds in rupture zones are first buckled whilst under tension from a configuration with angular rigidity to one without, and subsequently pulled apart. The comparison of the distribution of yield bending moment and tensile forces for two shear rates further suggested that the relative importance of bending and tension in aggravated failures is shifted strongly towards bending for decreasing shear rates. We did not find a single failure where bending was not involved at all, whereas pure bending failures and failures of bending in compression did occur. We therefore claim that bending is the major partner in the process of aggravated failure in fractal clusters with local angular rigidity for low shear rates where stresses are equilibrated over a significant length. We anticipate that this is due to the way a small tensile force can cause a large bending moment in a curvilinear beam. If we apply an elongational force F_e to the tips of the strand, we induce local bending moments of the order $\Gamma_b \approx F_e R_\perp$, where the lever $R_\perp$ is the distance of a bond perpendicular to the line joining the tips of the strand. It would follow that the importance of bending should increase for a lower initial area fraction ϕ_a and loopless fractals, where the elastic backbones become more tenuous than was the case in our aggregates.

The reported scaling theory assumed constancy of the compliance exponent Z_c. However, buckling failure occurs throughout the region of stress buildup, which softens the structure (increasing Z_c). This we believe leads to the deviations from the power law on approach to the yield stress. Figure 12 shows a stress strain curve for the two $N_t = 1058$ aggregates, where the softening of the second aggregate is especially evident. Moreover, small kinks in the curves we believe are associated with buckling events during the stress buildup. These nonlinear effects associated with the aggravated failures complicate the application of a simple yield criterion and may explain the failure of the single yield criterion to fit the data of Fig. 8(a). Buscall *et al.* [6] have similarly attributed softening before the yield point in polystyrene gels to

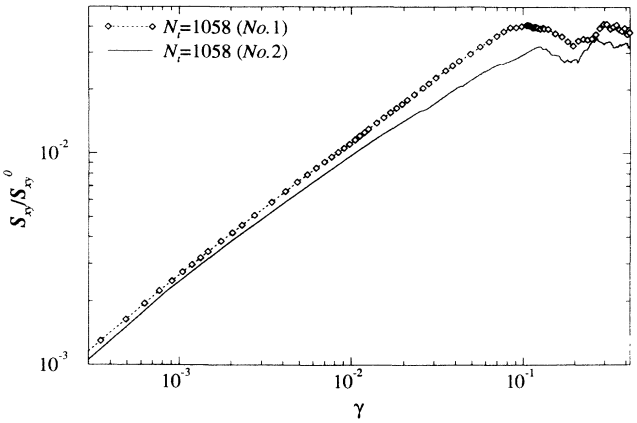

FIG. 12. Interparticle shear stress $\mathbf{S}_{xy}/\mathbf{S}^0_{xy}$ vs strain γ on a log-log scale for both aggregates with N_t=1058 (see legend) for a very low shear rate, $W = 1.526 \times 10^{-3}$—the effect of buckling preyield stress is well observable for this shear rate where stress concentration is very strong. The small kinks close to $\gamma \approx 2, 3, 7 \times 10^{-2}$ on the curve of $N_t = 1058$ (No. 2), we interpret as the buckling of bb(3) bonds which soften the structure. Hence the slope of the stress-strain curve becomes lower, i.e., the elastic compliance exponent Z_c is shifted to higher values.

rupture events, postulating that a significant fraction of broken bonds must be accumulated before the apparent yield. They also noted that this could explain their experimental observation of incomplete elastic recovery for deformations below the yield point.

For weak gels Brownian motion may play a role at the lower W values studied in the Stokesian simulations, and we have made a limited investigation of this. In the case of the thermally stable aggregates of the potential (1), Brownian motion influences the breakup of the gel in two ways. It acts as a "catalyst," breaking bonds which would not have been broken by systematic forces alone, and it also helps to equilibrate the stresses faster. It did not, however, influence the scaling laws in a systematic way, besides enhancing the fluctuations in the stress.

Hydrodynamic interactions were neglected, which in real systems may play a significant role. Dense regions of the aggregate will screen the flow field of the solvent into the less dense regions—this may enhance bending moments and forces on the outer edges of strong blobs and enhancing the flow forces acting within weak junctions. Furthermore, density variations will couple to local viscosity variations which will alter the drag coefficient significantly away from the Rouse form assumed in Sec. II. A full understanding awaits efficient hydrodynamic simulations.

V. CONCLUSIONS

A simple scaling theory predicts power laws governing the transient response of a colloid aggregate to applied shear rates, for rates such that the relevant length scales fall within the fractal regime of the aggregate. These power laws were found to describe the results of simula-

tion models in monolayers. The compliance exponent for two-dimensional fractal aggregates with angular rigidity of the colloid bond and loops on all scales we estimate from the largest aggregates studied to be in the range 1.1–1.3. The rupture of these networks was found to be complex and for the model used here involved a mode of aggravated failure—bending failure under tension.

ACKNOWLEDGMENTS

A.H.L.W. would like to acknowledge gratefully financial support by the Deutsche Akademische Austauschdienst (DAAD). J.R.M. is supported by a U.K. Department of Trade and Industry (DTI) Link Project cofunded by DTI, Unilever, ICI, and Schlumberger.

[1] J. Eisenlauer and E. Killmann, J. Colloid Interface Sci. **74**, 108 (1980).
[2] E. Dickinson, *An Introduction to Food Colloids* (Oxford University Press, New York, 1992).
[3] R. Wessel and R. C. Ball, Phys. Rev. A **46**, R3008 (1992).
[4] P. D. Patel and W. B. Russel, Colloids Surf. **31**, 355 (1988).
[5] M. Chen and W. B. Russel, J. Colloid Interface Sci. **141**, 564 (1991).
[6] R. Buscall, P. D. A. Mills, and G. E. Yates, Colloids Surf. **18**, 341 (1986); R. Buscall, J. I. McGowan, P. D. A. Mills, R. F. Stewart, D. Sutton, L. R. White, and G. E. Yates, J. Non-Newt. Fluid Mech. **24**, 183 (1987); R. Buscall, P. D. A. Mills, J. W. Goodwin, and D. W. Lawson, J. Chem. Soc. Faraday Trans. 1 **84**, 4249 (1988).
[7] R. Buscall, J. I. McGowan, and A. J. Morton-Jones, J. Rheol. **37**, 621 (1993) (and references therein).
[8] T. Annable, R. Buscall, R. Ettelaie, and D. Whittlestone, J. Rheol. **37**, 695 (1993).
[9] R. J. Hunter and J. Frayne, J. Colloid Interface Sci. **76**, 107 (1980).
[10] M. Doi and D. Chen, J. Chem. Phys. **90**, 5271 (1989); D. Chen and M. Doi, *ibid.* **91**, 2656 (1989).
[11] A. A. Potanin, J. Chem. Phys. **96**, 9191 (1992); J. Colloid Interface Sci. **157**, 399 (1993).
[12] J. R. Melrose and D. M. Heyes, J. Colloid Interface Sci. **157**, 227 (1993); J. R. Melrose, Europhys. Lett. **19**, 51 (1992); Phys. Rev. A **44**, R4789 (1991).
[13] Y. Kantor and I. Webman, Phys. Rev. Lett. **52**, 1891 (1984).
[14] P. Meakin, in *On Growth and Form*, edited by H. E. Stanley and N. Ostrowsky (Martinus Nijhoff, Dordrecht, 1986), p. 111ff (and references therein).
[15] S. Asakura and F. Oosawa, J. Chem. Phys. **22**, 1255 (1954); J. Polym. Sci. **33**, 183 (1958).
[16] J. F. Joanny, L. Leibler, and P. G. de Gennes, J. Polym. Sci. Polym. Phys. Ed. **17**, 1073 (1979).
[17] W. B. Russel, D. A. Saville, and W. R. Schowalter, *Colloidal Dispersions* (Cambridge University Press, Cambridge, 1989), Chap. 8.
[18] P. Walstra and T. van Vliet, in *Food, Polymer and Gel Colloids*, edited by E. Dickinson (The Royal Society of Chemistry, Cambridge, 1982), p. 369ff.
[19] Y. Kantor and T. A. Witten, J. Phys. (Paris) **45**, L676 (1984).
[20] R. C. Ball, Physica D **38**, 13 (1989).
[21] P. B. Warren, Ph.D. thesis, University of Cambridge, 1990.
[22] R. J. Hunter, *Foundation of Colloid Science Vol. II* (Clarendon, Oxford, 1989), Chap. 18.
[23] G. Bossis, A. Meunier, and J. F. Brady, J. Chem. Phys. **94**, 5064 (1991).
[24] Z.-Y. Chen, J. M. Deutch, and P. Meakin, J. Chem Phys. **80**, 2982 (1984); Z.-Y. Chen, P. C. Neakliem, and P. Meakin, *ibid.* **89**, 5887 (1988).
[25] F. E. Torres, W. B. Russel, and W. R. Schowalter, J. Colloid Interface Sci. **143**, 51 (1991).
[26] M. P. Allen and D. J. Tildesley, *Computer Simulation of Liquids* (Oxford University Press, Oxford, 1987), p. 225ff.
[27] D. M. Heyes, J. Non-Newt. Fluid Mech. **27**, 47 (1988).
[28] L. Marshall, C. F. Zukowski IV, and J. W. Goodwin, J. Chem. Soc. Faraday Trans. 1 **85**, 3785 (1989).